

Cylindrical Acoustic Gas Thermometry

Li Xing¹, Xiao-Juan Feng^{1,*}, Ming-Hao Si^{1,2}, Jin-Tao Zhang^{1,*},

Hong Lin¹, Keith A. Gillis³, Michael R. Moldover³

¹ National Institute of Metrology, Beijing 100029, People's Republic of China

² Tsinghua University, Beijing 100084, People's Republic of China

³ National Institute of Standards and Technology, Gaithersburg, MD 20899-8360,
United States of America

Authors to whom correspondence should be addressed: fengxj@nim.ac.cn;
zhangjint@nim.ac.cn

Abstract: We review recent determinations of the Boltzmann constant k_B and the differences $T-T_{90}$ that used cylindrical acoustic gas thermometry (c-AGT). These determinations measured the acoustic resonance frequencies of argon gas enclosed by metal-walled, cylindrical cavities. (Here, T is the thermodynamic temperature and T_{90} is the temperature measured on the International Temperature Scale ITS-90.) In the range 234 K to 303 K, the standard uncertainty of c-AGT ranges from $1.9 \times 10^{-6} T$ to $2.6 \times 10^{-6} T$. This uncertainty is much smaller than the errors in ITS-90; therefore, c-AGT can help improve ITS-90. Moreover, we are extending c-AGT up to 1358 K. With increasing temperatures, c-AGT becomes advantageous relative to AGT based on quasi-spherical cavities because long cylindrical cavities: (1) naturally fit into cylindrical heat pipes or multi-shelled thermostats, (2) provide the immersion required by transfer temperature standards such as long-stemmed platinum resistance thermometers, and (3) have more useful, low-frequency acoustic resonances. In preparation for high-temperature c-AGT, we identified suitable materials for fabricating cylindrical cavities and we developed techniques for measuring acoustic resonance frequencies using sources and detectors outside the high-temperature thermostat. We also considered alternative test gases and optimal dimensions of cavities.

This is the author's peer reviewed, accepted manuscript. However, the online version of record will be different from this version once it has been copyedited and typeset.
PLEASE CITE THIS ARTICLE AS DOI: 10.1063/1.50139385

29 **1. Introduction**

30 During the last 100+ years, the international thermometry community has
31 repeatedly refined consensus temperature scales to approximate the thermodynamic
32 temperature T as accurately as possible. The most recent consensus scale is the
33 International Temperature Scale of 1990 (abbreviated ITS-90)^[1]. Temperatures on ITS-
34 90 are denoted T_{90} ; they are disseminated by many National Metrology Institutes
35 (NMIs), such as China's National Metrology Institute (NIM) and the USA's National
36 Institute of Standards and Technology (NIST). Acoustic gas thermometry (AGT),
37 relating the squared speed of sound and the thermodynamic temperature of a gas
38 according to the fundamental state equation, is the state-of-the-art primary method for
39 the determination of the Boltzmann constant^[2-4] and the differences $T - T_{90}$ ^[5-8]. Figure 1
40 displays the temperature differences $T - T_{90}$ between thermodynamic temperatures T
41 and the ITS-90, as deduced from post-1990 measurements of the speed of sound in
42 argon. The data from laboratories in five countries^[9-16] fall outside the gray shaded area
43 that bounds the uncertainty of ITS-90 (In this paper, uncertainties are one standard
44 uncertainty corresponding to a 68 % confidence level), as estimated by the developers
45 of ITS-90. Therefore, the speed-of-sound data imply ITS-90 has errors that can be
46 substantially reduced. Data from dielectric-constant gas thermometry below 273 K
47 confirm this implication^[17,18]. The speed-of-sound data imply the fractional errors in
48 T_{90} are approximately -30 parts per million near 173 K and $+30$ parts per million near
49 473 K. Near 273 K, the slope $dT/dT_{90} \approx 1.0001$; this implies that a perfect measurement
50 of the specific heat of any material using thermometers calibrated on ITS-90 will yield
51 a result that is 0.01 % larger than the true specific heat of that material near 273 K.

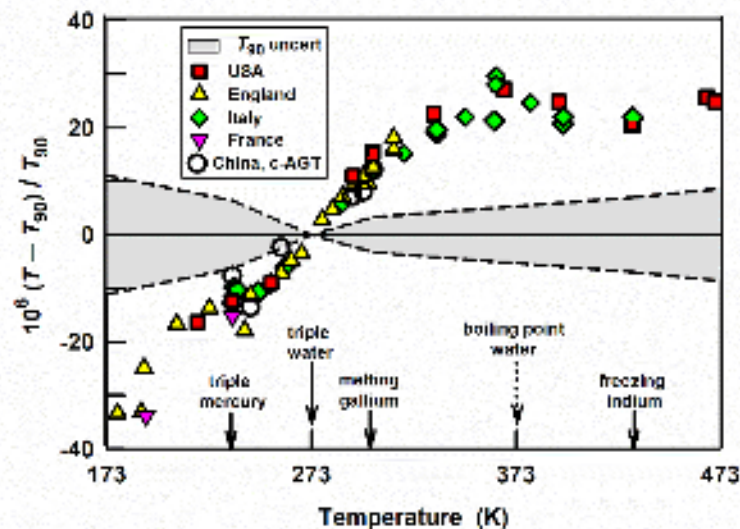


Fig. 1 Fractional differences ($\times 10^6$) between the thermodynamic temperature T and the International Temperature Scale of 1990 (ITS-90) as deduced from measuring the speed of sound since 1990. Arrows indicate the temperatures of four fixed points and the boiling point of water. The c-AGT data are consistent with the other acoustic data acquired using quasi-spherical cavities. Data sources: USA [9-11]; England [12,13]; Italy [14]; France [15]; China [16].

The international thermometry community is actively working to reduce the errors and uncertainties of ITS-90 at temperatures up to the copper point (1357.77 K), where $T - T_{90} \approx 52 \text{ mK}$ ^[19,20]. A significant part of this program is extending the techniques of acoustic gas thermometry (AGT) to temperatures above 430 K with low uncertainties. This review emphasizes the progress made in determining T from measurements of the acoustic resonance frequencies of argon gas enclosed by cylindrical cavities (c-AGT). With increasing temperatures, c-AGT becomes advantageous relative to q-AGT (quasi-spherical-cavity based AGT) because long cylindrical cavities^[21-25]: (1) naturally fit into cylindrical heat pipes or multi-shelled thermostats, (2) provide the immersion required by transfer temperature standards such as long-stemmed platinum resistance thermometers, and (3) have more useful, low-frequency acoustic resonances.

In Fig. 1, the scatter of the c-AGT data is larger than the scatter of the other speed of sound data that were acquired using spherical or quasi-spherical argon-filled cavities. Consistent with this observation, the c-AGT measurement of the Boltzmann constant k_B had a larger uncertainty than q-AGT measurements of k_B ^[26-30]. The larger scatter in the c-AGT resulted from the inconsistent values of k_B obtained from the various

This is the author's peer reviewed, accepted manuscript. However, the online version of record will be different from this version once it has been copyedited and typeset. PLEASE CITE THIS ARTICLE AS DOI: 10.1063/1.5019938

75 resonance modes of the argon in a given cylindrical cavity^[30]. As discussed below, such
76 inconsistent values could result from imperfect modeling of the cavity's shape
77 (including corners, ducts that admit gas, microwave cables, and so on) and/or imperfect
78 modeling of the elastic coupling of the cavity's walls (the shell of the cavity) to the
79 oscillations of the gas within the cavity^[31-33]. Shape-generated inconsistencies will have
80 a very weak temperature dependence; therefore, they will generate only small
81 uncertainties when measuring temperature ratios T/T_{ref} (Here T is a measured
82 temperature and T_{ref} is a fixed, known reference temperature near ambient temperature).
83 In contrast, inconsistencies generated through elastic coupling will lead to large
84 uncertainties in T/T_{ref} because such couplings have a strong temperature dependence.
85 Because the frequencies of the gas resonances increase as $T^{1/2}$ and the frequencies of
86 the shell's resonances decrease as the shell's elastic constants decrease, shell frequencies
87 and gas frequencies will couple strongly when the frequencies appear to cross. Recent
88 measurements at the National Physical Laboratory (NPL) in 2020^[19] displayed the
89 mode-dependent, inconsistent values of T/T_{ref} determined from 27 c-AGT modes with
90 $T_{\text{ref}} = 323$ K and $T = 429$ K. For most of the 27 modes, the deviations at T and T_{ref} are
91 nearly independent of temperature. For a few modes, a strong temperature dependence
92 is visible. The similar conclusion is also found in the measurement from NIM in 2016^[25].

93 In preparation for high-temperature c-AGT, we identified suitable materials for
94 fabricating cylindrical shells and we developed techniques for measuring acoustic
95 resonance frequencies using sources and detectors outside the high-temperature
96 thermostat. We also considered alternative test gases and optimal dimensions of cavities.

97 **2. General Principle**

98 **2.1 Absolute primary c-AGT**

99 Absolute primary thermometry is the procedure to determine the thermodynamic
100 temperature of a well-defined system by measuring some independent quantities using
101 a clearly stated equation and fundamental constants^[34,35]. AGT is one of the absolute
102 thermometric methods, which operates to form specific acoustic resonances in a

103 resonator. We have applied fixed-length cylindrical cavities as acoustic resonators, and
104 named such a procedure c-AGT.

105 Given a weak pressure wave in the longitudinal direction applied to a dilute gas
106 confined in the cylindrical cavity, the pressure creates a resonance at mode l , when the
107 half wavelengths $\lambda/2$ match the resonant condition, that is $l \cdot (\lambda/2) = L$, $l=1, 2, \dots, n$. The
108 integer l is defined as the mode number. The kinetic energy of ideal gas particles is
109 equal to the thermal energy according to the equipartition theorem^[30], which can be
110 expressed as

$$111 \quad \frac{1}{2}mv^2 = \frac{3}{2} \frac{m}{\gamma_0} \left(\frac{\partial p}{\partial \rho} \right)_s = \frac{3}{2} k_B T, \quad (1)$$

112 where v is the root-mean-square (RMS) velocity of an atom of mass m , ρ is the mass
113 density of the gas, p is the gas pressure, and T is the thermodynamic temperature of the
114 gas. γ_0 is the ideal gas heat-capacity ratio with $\gamma_0 \equiv C_{p0}/C_{v0}$, and the ratio is exactly 5/3
115 for a monatomic gas. The subscript 'S' labels the state at a constant entropy. Using a
116 thermodynamic relationship to rewrite the pressure derivative in terms of the squared
117 speed of sound, w_0^2 , Eq. (1) is formulated into the principal equation for c-AGT,

$$118 \quad w_0^2 = \left(\frac{\partial p}{\partial \rho} \right)_s = \frac{\gamma_0 k_B T}{m}. \quad (2)$$

119 The Boltzmann constant k_B can be described by

$$120 \quad k_B = \frac{w_0^2 M}{T \gamma_0 N_A}, \quad (3)$$

121 where N_A is the Avogadro constant^[36] and M is the average molar mass of the gas. Real
122 monatomic gases deviate from the ideal gas by the existence of interatomic collisions.
123 The correction to Eq. (2) created by such a deviation is given by the acoustic virial
124 expansion for a dilute monatomic gas, that is

$$125 \quad w^2 = A_0 + A_1(T)p + A_2(T)p^2 + A_3p^3 + A_{-1}(T)p^{-1} + \dots, \quad (4)$$

126 where w^2 is the squared speed of sound of the gas and $A_0 = w_0^2$. A_1 is closely related to
127 the second acoustic virial coefficient, which represents the deviation caused by atomic

128 pair collisions. Moreover, A_2 and A_3 are related to the third and fourth acoustic virial
129 coefficients generated by collisions among three and four atoms, respectively. A_{-1}
130 represents the imperfect energy and momentum accommodation between the gas and
131 cavity walls^[37].

132 The speed of sound w can be derived from an unperturbed resonant frequency f_l^0
133 at the non-degenerate longitudinal acoustic modes l , which are preferably used in c-
134 AGT, the length L of a cylindrical resonator at pressures p and a chosen isotherm T .
135 The relation to retrieve the speed of sound w is

$$136 \quad w = \frac{2f_l^0 L}{l}. \quad (5)$$

137 2.2 Relative primary c-AGT

138 Relative primary AGT determines the ratio of two thermodynamic temperatures
139 from measurements of the ratios of sound speeds on the chosen and the reference
140 isotherms^[38]. Compared to absolute primary AGT, the temperature-independent errors
141 are anticipated to be reduced by ratio calculations. Normally, if the triple point of water
142 temperature T_{TPW} is used as the reference, the unknown T is proportional to the
143 reference according to Eq. (4)^[16],

$$144 \quad T = T_{\text{TPW}} \frac{A_0(T)}{A_0(T_{\text{TPW}})} = T_{\text{TPW}} \frac{\lim_{p \rightarrow 0} [f_l^0(T, p) \cdot L(T, p)]^2}{\lim_{p \rightarrow 0} [f_l^0(T_{\text{TPW}}, p) \cdot L(T_{\text{TPW}}, p)]^2}. \quad (6)$$

145 2.3 Retrieval of unperturbed parameters

146 In practice, the acoustic resonances in a cylindrical resonator are perturbed by the
147 elastic response of the shell and endplates, the viscosity and thermal conductivity of the
148 sample gas, interactions between the transducers and the sample gas, and gas-filled
149 ducts. The imperfections appear as non-zero admittances and create perturbations on
150 acoustic resonances formed in the cylindrical cavity. The effects on the resonance
151 frequencies are approximated by first-order perturbation theory, and the higher order
152 effects are neglected. Thus, the unperturbed resonant frequency f_l^0 at mode l is derived
153 from its measurement f_l by

$$154 \quad f_l^0 = f_l - \sum_i \Delta f_i, \quad i=1,2,\dots, \quad (7)$$

155 where subscript i denotes the given imperfection effects, according to their different

156 mechanisms forming non-zero admittances. They are generally catalogued into four
157 types caused by a) boundary layers, b) the motion of the shell, c) acoustic transducers,
158 and d) the gas fill ducts^[32,39,40]. In order to acquire accurate measurement results, the
159 calculation and correction of the perturbation effects are necessary.

160 The effects of boundary layers contribute the largest perturbation and are mainly
161 generated by dissipation during each acoustic cycle. Velocity gradients are formed by
162 viscous boundary layers near the cylindrical shell surface because of the viscosity of
163 sample gas. Similarly, a temperature gradient is formed through a thermal boundary
164 layer due to the finite thermal conductivity of the gas. These perturbations
165 simultaneously disperse and dissipate the acoustic energy. In addition, a thermal
166 boundary layer is formed near the endplates and imposes a similar perturbation effect.
167 The dispersion decreases resonance frequencies, while the dissipation broadens
168 resonance profiles.

169 According to first-order perturbation theory, the acoustic boundary layer alters the
170 resonance frequency and increases the energy dissipation. Viscous damping shifts the
171 resonance frequency for the longitudinal modes by the fractional amount^[32]

$$172 \frac{(\Delta f_l)_v}{f_l^0} = -\frac{1}{2a}(\delta_v - 2l_v), \quad (8)$$

173 where a is the radius of the cylindrical cavity. l_v is the pressure-dependent viscous
174 accommodation length, and δ_v is the viscous penetration length, which can be
175 expressed by

$$176 l_v = \frac{\eta}{p} \sqrt{\frac{\pi RT}{2M}} \frac{2-h_v}{h_v}, \quad (9)$$

$$177 \delta_v = \sqrt{\frac{\eta}{\pi f_l \rho}}, \quad (10)$$

178 where $R \equiv k_B N_A$ is the molar gas constant, h_v is the viscous accommodation
179 coefficient, and η is the shear viscosity at the working pressure and temperature. The
180 half-width $(g_l)_v$ of acoustic resonances caused by the viscous boundary layer is given
181 by

$$182 \quad \frac{(g_l)_v}{f_l^0} = \frac{\delta_v}{2a} = \frac{1}{2a} \sqrt{\frac{\eta}{\pi f_l \rho}}. \quad (11)$$

183 The effect of the thermal boundary layer on the resonance frequency can be
184 described by^[32]

$$185 \quad \frac{(\Delta f_l)_{th}}{f_l^0} = -\frac{\gamma-1}{2a} \left[(\delta_{th} - 2l_{th}) \left(1 + \frac{2a}{L} \right) - \frac{\kappa}{\kappa_{shell}} \delta_{th,shell} - \frac{2a}{L} \frac{\kappa}{\kappa_{endplate}} \delta_{th,endplate} \right]. \quad (12)$$

186 Here the subscripts “shell” and “endplate” represent the material properties, l_{th} is the
187 thermal accommodation length, and δ_{th} is the thermal penetration length, given by

$$188 \quad l_{th} = \frac{\kappa}{p} \sqrt{\frac{\pi MT}{2R}} \frac{2-h_{th}}{h_{th}} \frac{1}{C_{V,m}/R+0.5}, \quad (13)$$

$$189 \quad \delta_{th} = \sqrt{\frac{\kappa}{\pi f_l \rho C_p}}, \quad (14)$$

190 where h_{th} is the thermal accommodation coefficient, whose value is approximately 1.0^[7],
191 $C_{V,m}$ is the molar specific heat at constant volume of the gas, and κ is the thermal
192 conductivity of the gas. The half-widths $(g_l)_{th}$ caused by the thermal boundary layer
193 are expressed by

$$194 \quad \frac{(g_l)_{th}}{f_l^0} = \frac{\gamma-1}{2a} \left[\delta_{th} \left(1 + \frac{2a}{L} \right) - \frac{\kappa}{\kappa_{shell}} \delta_{th,shell} - \frac{2a}{L} \frac{\kappa}{\kappa_{endplate}} \delta_{th,endplate} \right]. \quad (15)$$

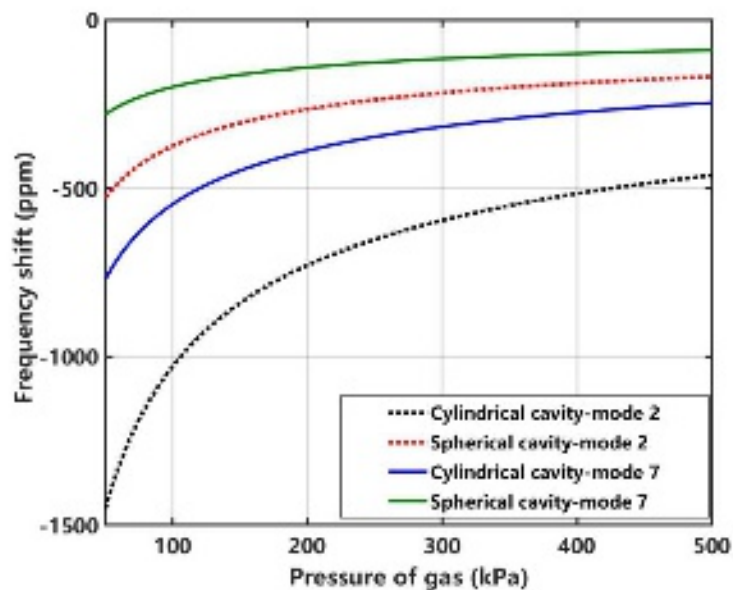
195 The attenuation of acoustic oscillations includes dissipation in the whole cavity
196 because of the viscosity and the thermal conductivity of the gas, which contributes an
197 additional term $(g_l)_{bulk}$ to the half-width^[7] given by

$$198 \quad \frac{(g_l)_{bulk}}{f_l^0} = \left(\frac{\pi f}{w} \right)^2 \left[\frac{4}{3} \delta_v^2 + (\gamma-1) \delta_{th}^2 \right]. \quad (16)$$

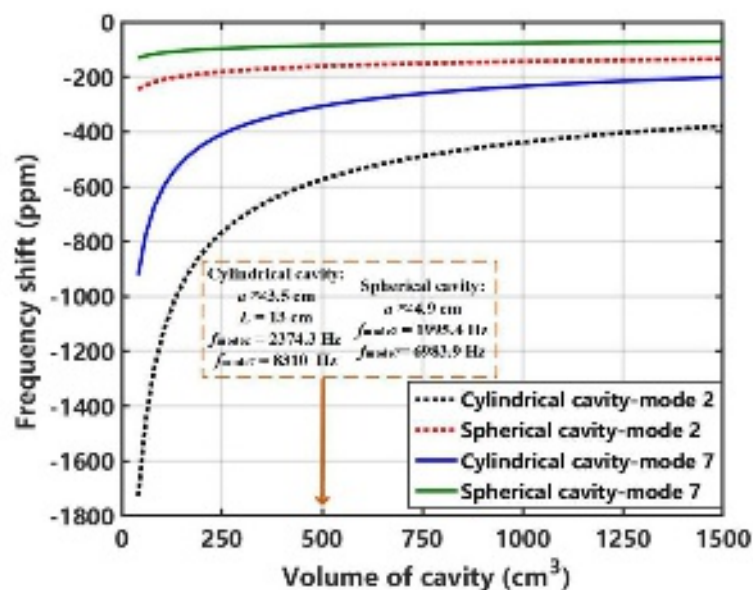
199 The equations above, combined with experimental results, show the boundary
200 layer effects are the largest perturbations for c-AGT^[30]. According to Ref. [38],
201 dissipation of radial modes in a spherical cavity is mainly due to the thermo-acoustic
202 boundary layer in the gas; there is basically no effect of the viscous boundary layer. The
203 frequency shift and the halfwidth due to thermal and viscous boundary layers (except
204 for the small accommodation correction) have the same magnitude but opposite sign:

This is the author's peer reviewed, accepted manuscript. However, the online version of record will be different from this version once it has been copyedited and typeset. PLEASE CITE THIS ARTICLE AS DOI:10.1063/1.503381

205 $(\Delta f_l)_v \approx -(g_l)_v$ and $(\Delta f_l)_{th} \approx -(g_l)_{th}$. To clarify the difference between cylindrical and
 206 spherical cavities with the same volume, we computed the boundary layer effects for
 207 both geometries as shown in Fig. 2. The parameters of argon^[7,41,42] are applied in the
 208 calculation, and the temperature is set at T_{TPW} . The comparison results indicate that the
 209 boundary layer effects for longitudinal modes of a cylindrical cavity are 2 to 3 times
 210 larger than for the radial modes of a spherical cavity of equal volume, and the length of
 211 the cylindrical cavity is equal to diameter of the spherical cavity. This is the main reason
 212 that restricts the application of cylindrical cavity for AGT. Moreover, the frequency
 213 shift and half-width decrease with the increase of gas pressure. When the pressure is
 214 larger than ~ 300 kPa, the impact of boundary layers is small and has a weak pressure
 215 dependence. The calculation results from boundary layers for different shell radii are
 216 shown in Fig. 3 with the length L of the cylindrical cavity fixed at 13 cm, which affects
 217 the value of the resonant frequency. The gas pressure is 505 kPa and the temperature is
 218 T_{TPW} in the calculation. As the volume of the cavity increases, the effect of the boundary
 219 layer is reduced, especially for the cylindrical cavities. When the volume is larger than
 220 1000 cm^3 , the impact is almost minimized and unchanged in the calculation.



221
 222 Fig. 2 Comparison of frequency shift from boundary layers between spherical and cylindrical
 223 cavities with the same volume at about 400 cm^3 under different gas pressures (spherical
 224 resonator $a \approx 4.57 \text{ cm}$, cylindrical cavity $a = 4 \text{ cm}$, $L = 8 \text{ cm}$).



225
226
227

Fig. 3 Comparison of frequency shift from boundary layers between spherical and cylindrical cavities ($L=13$ cm) with the same volume under different shell radius.

228

3. Measurement of the Boltzmann Constant

229

3.1 Determinations of the Boltzmann constant

230

Since 2009, we have implemented absolute primary c-AGT for the determination of the Boltzmann constant. Our work is an independent complement to measurements by others using AGT with spherical and quasi-spherical resonators. We alternatively implemented absolute primary c-AGT with single cylindrical resonators^[24,30] and two cylindrical cavities creating a virtual c-AGT^[43]. Seven independent cases were performed using argon as the sample gas. Except for the difference between procedures of single cavity and virtual cavity, the seven studies further differed from each other by the length of cylindrical cavities, the materials forming cylindrical shells and endplates, as well as the procedure measuring cylinder lengths. We summarize the determinations of the constant in Table 1.

231

232

233

234

235

236

237

238

239

240

Table 1. Differences among seven determinations of k_B with cylindrical acoustic resonators

Case	Year	Inner length (mm)	Result for k_B ($\times 10^{23}$ J/K)	Materials of shells and endplates	Filling gas (argon)	Method of measuring cylinder lengths
1 ^[32]	2009-2010	130	1.380650(11)	Bearing steel and quartz endplates	BIP	Coordinate measuring machine and two-color interferometry

This is the author's peer reviewed, accepted manuscript. However, the online version of record will be different from this version once it has been copyedited and typeset.

PLEASE DO NOT DISTRIBUTE THIS MANUSCRIPT
DOI: 10.1063/1.5131885

241
242
243
244
245
246
247
248
249
250
251
252
253
254
255

2	2010-2011	65	1.3806470(90)	Bearing steel and quartz endplates	BIP	Two-color interferometry
3	2011	65/130	1.3806478(33)	Bearing steel and quartz endplates	BIP	Two-color interferometry
4 ^[33]	2013	80	1.3806498(46)	Stainless steel and quartz endplates	BIP-Plus	Two-color interferometry
5 ^[33]	2013	80	1.3806460(53)	Stainless steel and quartz endplates	BIP, BIP-Plus	Two-color interferometry
6 ^[43]	2015	80/160	1.3806486(29)	Stainless steel and quartz endplates	BIP-Plus	Two-color interferometry
7 ^[30]	2017	80	1.3806483(58)	Oxygen free copper	BIP-Plus	Microwave resonance

Among the determinations, the first six were performed on cylindrical cavities made of bearing steel or stainless steel. The cavities shared the identical inner diameter of 80 mm. The lengths varied from 65 mm to 160 mm. The endplates were made of quartz glass for realization of the laser interferometry for measuring the resonator's lengths. The endplates between the resonators of Case 4 and Case 5 were interchanged, so that the measurement results of k_B were different. The seventh measurement used a cylindrical cavity made of oxygen-free copper and used microwave resonances to measure the resonator's length and radius to determine the cavity's volume^[44]. Figure 4 compares the seven determinations with their uncertainties with the value of k_B fixed by CODATA 2017^[26] They agree within the measurement's uncertainty. The detailed source of the measurement uncertainty can be found in Ref.[30]. For each resonator, the largest uncertainty source is the inconsistency between modes with details given in Sec. 3.5. Case 3 and Case 6 using the virtual cylindrical resonators, which are drawn with dashed lines, have small uncertainties because the mode inconsistency is ignored in our analysis.

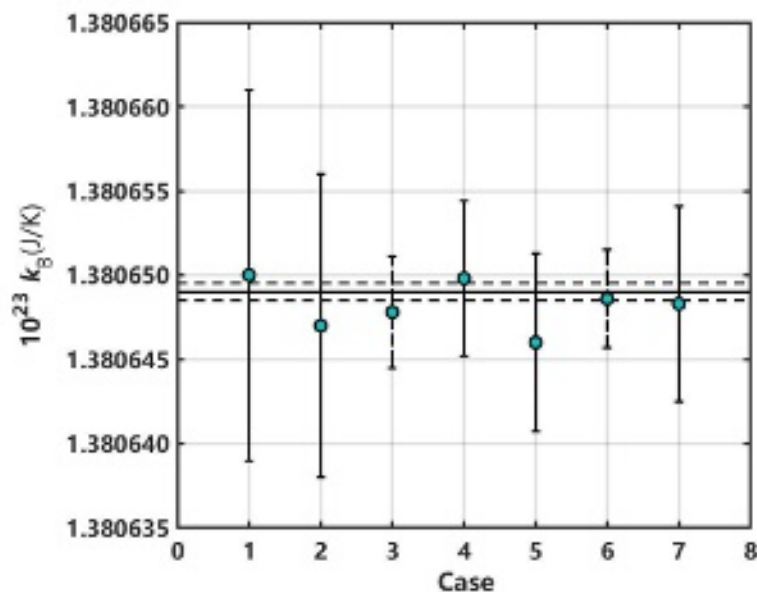


Fig. 4 Seven measurement results of k_B from c-AGT compared with CODATA 2017^[26]

3.2 Pressure dependence of the speed of sound in argon.

Our c-AGT measurements determine the pressure-dependent speed of sound $w^2(p, T)$ in argon on isotherms. In this section, we compare our measured pressure dependence with literature values determined using spherical cavity resonators. (See Figs. 5 and 6.) As indicated by Eq. (4), we expressed $w^2(p, T)$ as a power series of the pressure p . Others have expanded w^2 as power series of the molar density ρ or of the scaled pressure $p/(RT)$, which also has the units of density. Each of these expansions has been called an "acoustic virial series" and the temperature-dependent expansion coefficients have been called "acoustic virial coefficients" typically denoted as $\beta_a(T)$, $\gamma_a(T)$, $\delta_a(T)$, *etc.* To minimize confusion, we define our expansion coefficients by

$$\beta_{a,\text{press}} = RT \frac{A_1}{A_0} \quad \text{and} \quad \gamma_{a,\text{press}} = RT \frac{A_2}{A_0}, \quad (17)$$

where the subscript "press" identifies the expansion variable.

According to Eq. (17), $\beta_{a,\text{press}}$ and $\gamma_{a,\text{press}}$ can be retrieved from measurements of A_0 , A_1 and A_2 . However, compliance of the cylinder's walls perturbs the resonant frequencies by a linear function of the pressure with a mode-dependent coefficient; therefore, $\beta_{a,\text{press}}$ has an apparent mode dependence. We determined $\beta_{a,\text{press}}$ and $\gamma_{a,\text{press}}$ from averages over all the measured modes. During several determinations of the Boltzmann constant, we conducted c-AGT at T_{TPW} in its absolute mode. Our results for

276 k_B , $\beta_{a,\text{press}}$, and $\gamma_{a,\text{press}}$ at T_{TPW} are listed in Table 2. They are compared with results
277 obtained using spherical and quasi-spherical resonators in Figs. 5(a) and 5(b).

278 Table 2. Molar mass M and acoustic virial coefficients of argon at T_{TPW} determined by AGT

Case	Year	M (g mol ⁻¹)	$\beta_{a,\text{press}}$ (cm ³ mol ⁻¹)	$\gamma_{a,\text{press}}$ (cm ³ mol ⁻¹ MPa ⁻¹)
1	2009-2010	39.947 843±0.000 028 ^a	5.339	1.244
2	2010-2011	39.947 843±0.000 028 ^a	5.103	1.236
3	2011	39.947 843±0.000 028 ^a	5.400	1.284
4	2013	39.947 843±0.000 005 ^a	5.429	1.296
5	2013	39.947 810±0.000 010 ^{a,b}	5.500	1.270
6	2015	39.947 810±0.000 010 ^b	5.333	1.249
7	2017	39.947 794±0.000 031 ^b	5.290	1.213
8 ^[7]	1988	39.947 783±0.000 032	5.390	1.280
9 ^[9]	1999	39.947 781±0.000 032	5.401	1.275
10 ^[45]	2010	39.947 782±0.000 038	5.377	--
11 ^[22]	2013	39.947 816±0.000 017	5.438	1.219
12 ^[46]	2017	39.947 798±0.000 060	5.422	1.287

279 ^a BIP grade argon.

280 ^b BIP plus grade argon.

281 Our seven independent values of $\beta_{a,\text{press}}$ from Table 2 (Cases 1 to 7) have the
282 average $\langle\beta_{a,\text{press}}\rangle = 5.342$ cm³ mol⁻¹ with a fractional standard deviation of 2.19%. They
283 agree well with the typical results from AGT of spherical or quasi-spherical resonators,
284 which are indicated in Table 2 as Cases 8 to 12. From the same seven independent
285 experiments, we obtained $\langle\gamma_{a,\text{press}}\rangle = 1.256$ cm³ mol⁻¹ MPa⁻¹ with the fractional standard
286 deviation of 2.13%. The average value of the spherical resonators for Cases 8 to 12 is
287 1.265 cm³ mol⁻¹ MPa⁻¹ and the fractional standard deviation is 2.14%. In summary, the
288 c-AGT results for $\beta_{a,\text{press}}$ and $\gamma_{a,\text{press}}$ presented in Fig. 5 are consistent with the q-AGT
289 results from the literature.

This is the author's peer reviewed, accepted manuscript. However, the online version of record will be different from this version once it has been copyedited and typeset.

290

291

292

293

294

295

296

297

298

299

300

301

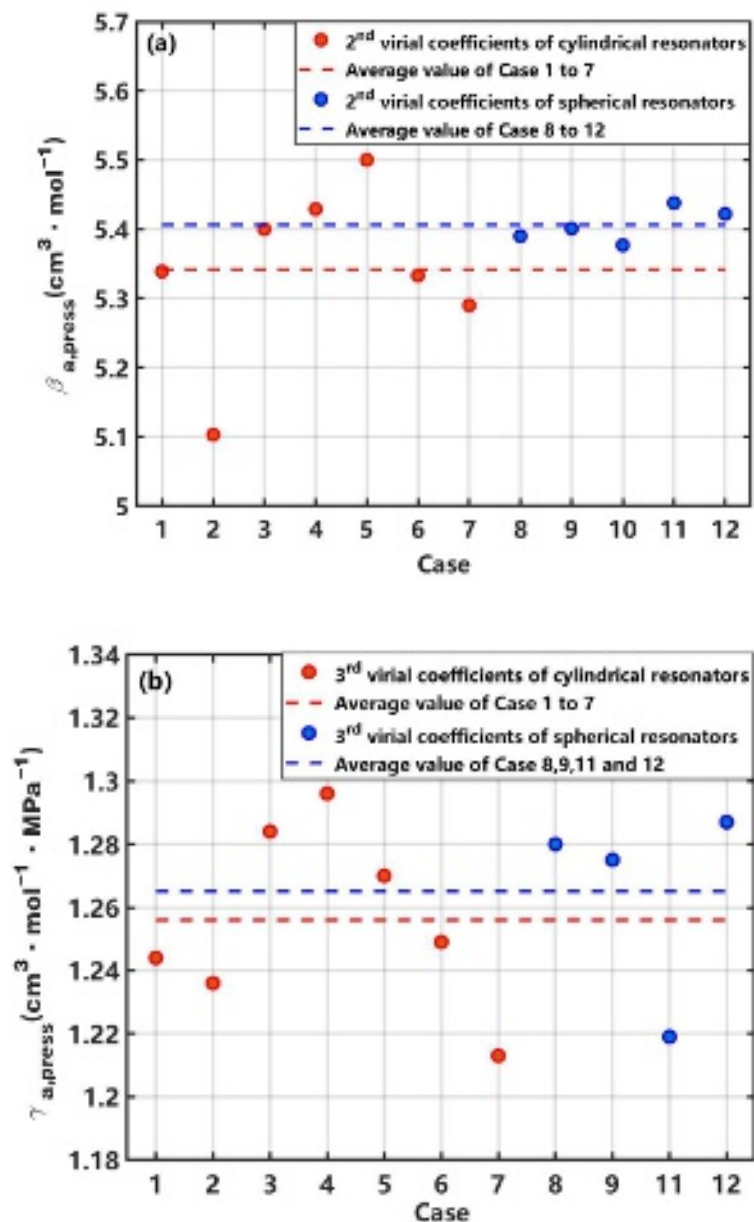


Fig. 5 The values of the 2nd and 3rd acoustic virial coefficients ($\beta_{a,press}$ and $\gamma_{a,press}$) of argon measured at T_{TPW} using cylindrical and spherical resonators.

In addition to our c-AGT work at T_{TPW} , we performed c-AGT in the relative mode at temperatures from 234 K to 303 K^[16] using argon as the thermometric gas; these measurements also generated values of $\beta_{a,press}$ and $\gamma_{a,press}$. Figures 6(a) and 6(b) show that these c-AGT values of $\beta_{a,press}$ and $\gamma_{a,press}$ are in good agreement with literature values obtained during AGT measurements that used spherical resonators^[9,14,47]. Moreover, the theoretical calculations of $\beta_{a,press}$ ^[38] and $\gamma_{a,press}$, as well as their expanded uncertainty ($k=2$) have been drawn in Figs. 6(a) and 6(b), respectively. The third acoustic virial coefficient expressed by density is given as^[38]

This is the author's peer reviewed, accepted manuscript. However, the online version of record will be different from this version once it has been copyedited and typeset.
PLEASE CITE THIS ARTICLE: DOI: 10.1063/1.5139385

$$\gamma_{a,\text{density}} = \frac{\gamma_0 - 1}{\gamma_0} [B + (2\gamma_0 - 1)T \frac{dB}{dT} + (\gamma_0 - 1)T^2 \frac{d^2B}{dT^2}]^2 + \frac{1 + 2\gamma_0}{\gamma_0} C + \frac{\gamma_0^2 - 1}{\gamma_0} T \frac{dC}{dT} + \frac{(\gamma_0 - 1)^2}{2\gamma_0} T^2 \frac{d^2C}{dT^2} \quad (18)$$

where B and C are the second and third density virial coefficients, respectively, which were calculated from Ref. [48]. The third acoustic virial coefficient can be transformed into a pressure expansion by

$$\gamma_{a,\text{press}} = \frac{(\gamma_{a,\text{density}} - B\beta_{a,\text{press}})}{RT}. \quad (19)$$

The uncertainty for the third acoustic virial coefficient in Fig. 6(b) was calculated from the uncertainties of B , $\beta_{a,\text{press}}$,^[38] and C , which was $40 \text{ cm}^6 \text{ mol}^{-2}$ roughly obtained from the absolute deviations of Fig. 3 in Ref. [48].

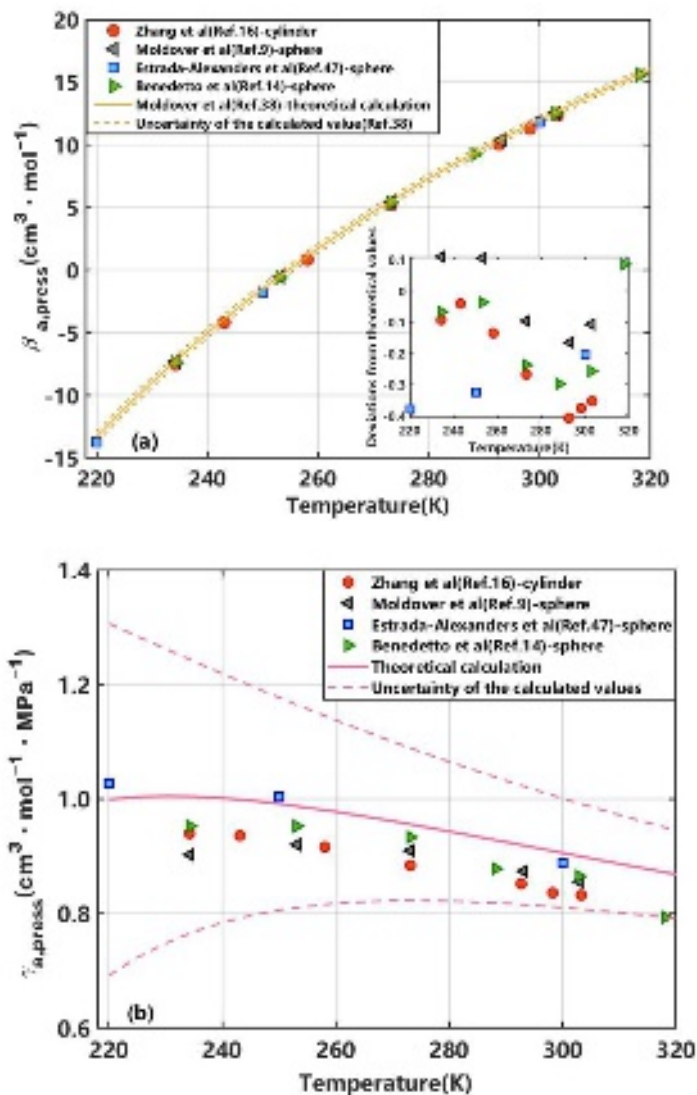


Fig. 6 Values of 2nd and 3rd acoustic virial coefficients $\beta_{a,\text{press}}$ and $\gamma_{a,\text{press}}$ measured using cylindrical and spherical resonators at different temperatures. The theoretical calculation of $\gamma_{a,\text{press}}$ and the expanded uncertainty of the calculated values are based on Eq.(21) from Ref. [48] and equations from supplement in Ref. [38].

316 3.3 Measurements of mechanical cross-talk of evacuated resonators

317 In order to select resonant modes of the gas that are less affected by the natural
318 vibration of the resonator's shell or by either electrical or mechanical cross-talk between
319 the acoustic source and acoustic detector, we scanned the acoustic source at frequencies
320 from 1 kHz to 10 kHz while the cavity was under vacuum at T_{TPW} . Both the acoustic
321 source and detector used in these works were piezoelectric transformer (PZT)
322 transducers, which were respectively built in the upper and lower endplates. The
323 acoustic transducer in endplates were designed with thin, well-machined diaphragms
324 and the transducers were bonded to the diaphragms with epoxy. Figure 7 shows the
325 detected signal for three cases:

- 326 (1) Case 4 (stainless steel shell, quartz endplates, $L=80$ mm),
- 327 (2) Case 7 (oxygen-free copper shell, oxygen-free copper endplates $L=80$ mm)
- 328 (3) Case 6 (stainless steel shell, quartz endplates, $L=160$ mm).

329 For these three cases, the detector's response was small at frequencies below 7 kHz.
330 Below 7 kHz, there was no overlap between the shell's natural vibrations and the gas's
331 resonances at pressures of 75 kPa and 150 kPa. Cases 4 and 6 both used resonators
332 made of stainless steel with quartz endplates, but they had different dimensions. The
333 detected signal was weaker in the longer resonator. Cases 4 and 7 both used resonators
334 with the same dimensions but made from different materials. Their different
335 performances were obvious above 8 kHz. The detected signal was much larger for the
336 oxygen-free copper resonator, whose endplates and bolts were also made of oxygen-
337 free copper. The vibration of transducers is more easily transmitted to the copper cavity
338 due to the different elastic moduli of copper and quartz endplates in Cases 4 and 6. In
339 summary, the natural vibration of resonators is mainly impacted by the materials of
340 shells and endplates; the resonator made of oxygen-free copper would transmit obvious
341 high-frequency vibration. The dimensions of the cylindrical resonator have little
342 influence on the variation of vibration. Moreover, we also measured the acoustic
343 spectrum of the resonator filled with argon. The measurements of acoustic resonance
344 of argon are easily affected by the resonator vibration in the high-frequency region. In
345 conclusion, the modes whose resonance frequencies are less than 7 kHz were suitable

346 for acoustic measurement in our experiments. However, because the signal-to-noise
347 ratio of the acoustic resonance of the (1,0,0) mode is usually lower and the perturbation
348 is also larger, we didn't use it in our determination.

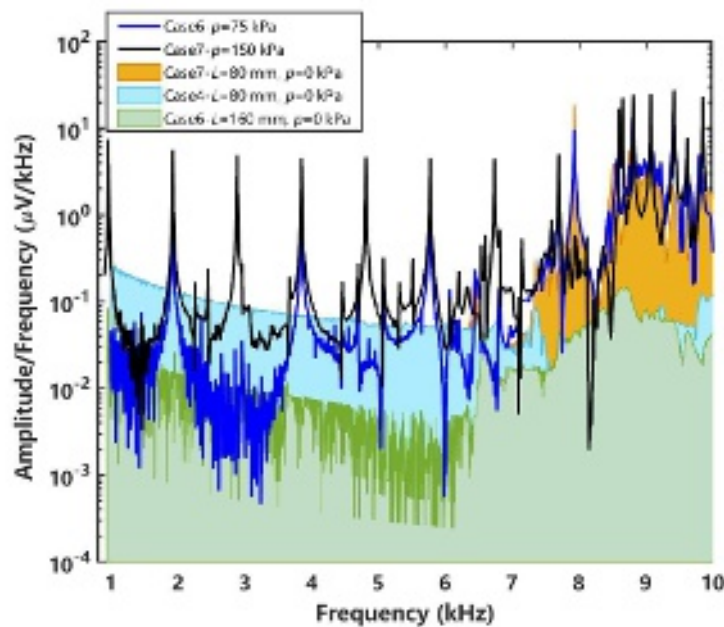


Fig. 7 Spectrum of different evacuated and gas-filled resonators.

3.4 Virtual cylindrical acoustic resonator

In order to minimize the perturbations of cavities' endplates containing transducers and/or ducts, we first proposed the concept of a virtual resonator through combining the resonance frequencies of two cylindrical cavities^[43]. The working equations of the speed of sound for virtual cylindrical resonator can be described as

$$w = \frac{2f_1 f_2 \Delta L_{12}}{l_1 f_2 - l_2 f_1} \left(1 - \frac{\delta L_{12}}{\Delta L_{12}} \right), \quad (20)$$

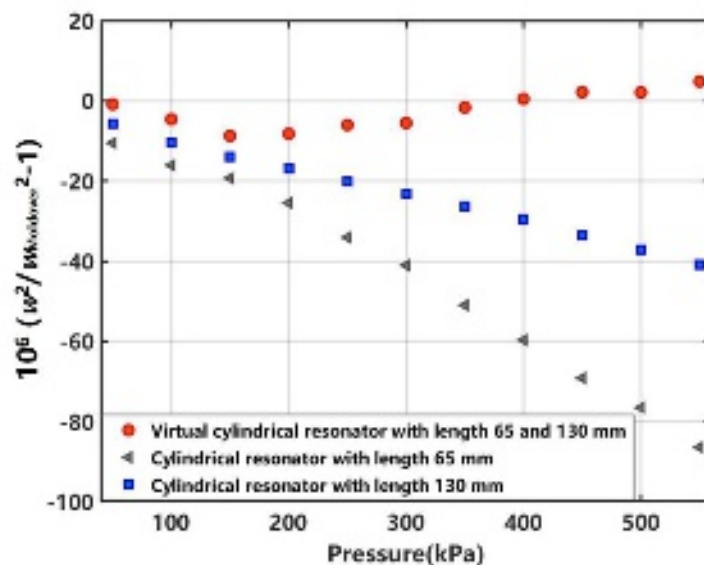
where f_1 and f_2 are the measured resonance frequencies of the two cavities in the virtual resonator with modes $l_1=2l_2$. The length of virtual resonator is $\Delta L_{12} = L_1 - L_2$ and has no endplates. L_1 and L_2 are the length of the two cavities. The small correction determined by the perturbations Δf_1 and Δf_2 can be expressed as

$$\frac{\delta L_{12}}{\Delta L_{12}} = \frac{L_1}{\Delta L_{12}} \frac{\Delta f_1}{f_1^{(0)}} - \frac{L_2}{\Delta L_{12}} \frac{\Delta f_2}{f_2^{(0)}}. \quad (21)$$

The lengths of the two resonators differ by a factor of two, and the cavities are operated at nearly identical longitudinal resonance frequencies for the non-degenerate

This is the author's peer reviewed, accepted manuscript. However, the online version of record will be different from this version once it has been copyedited and typeset. PLEASE CITE THIS ARTICLE AS DOI: 10.1063/1.5191971

364 longitudinal mode $l=2$ in the shorter cavity and for the mode $l=4$ in the longer cavity.
 365 Thus, the frequency-dependent admittances of the endplates can be eliminated to first
 366 order in Eqs. (20) and (21), so that the virtual resonator has a higher effective quality
 367 factor (Q) than the modes for either of the actual resonators. Moreover, the deviation of
 368 the speed of sound in the virtual cylindrical resonator can be suppressed with increased
 369 gas pressure. The comparison for the relative squared speed of sound deviations
 370 between virtual and real resonators is shown in Fig. 8. The deviation is calculated from
 371 the difference between the speed of sound obtained by our cylindrical cavity after
 372 correcting the non-ideal factors and the results of Moldover *et al.* in 1988^[7]. The
 373 absolute value of the deviation linearly increases with rising gas pressure in the real
 374 resonator. However, the deviation is nearly insensitive to the pressure in the virtual
 375 resonator. Thus, the virtual resonator suppresses the effect of the boundary layer and
 376 shell vibration, so that the measurement error of speed of sound is reduced. We
 377 measured k_B using two virtual cylinders with the results listed in Table 1 and Fig. 4.
 378 Both values have a good agreement with CODATA 2017^[26]. Because the effects from
 379 shell motion at high frequency limited the acoustic modes combinations for the virtual
 380 cylinder, we can only use one combination of acoustic modes. Nevertheless, the virtual
 381 cavity is very effective for the speed of sound measurement using c-AGT with less
 382 energy loss and frequency shift.



383

384 Fig. 8 The comparison for measurement deviation of speed of sound between virtual resonator
 385 and single resonators at T_{TPW} .

386 **3.5 Measurement Uncertainty**

387 The sources of measurement uncertainty of k_B mainly include measurements of
388 temperature, pressure, acoustic frequencies, cavity length, and molar mass, which have
389 been described in our published articles^[30,33]. According to our uncertainty analysis for
390 the seven independent measurements, the main uncertainty sources for c-AGT are from
391 the temperature measurement, random error from fitting isotherm data in A_0 , and
392 inconsistency among the measured modes. An assembly with a copper sleeve for the
393 standard capsule-type platinum resistance thermometer has been designed to promote
394 the stability of temperature measurement^[33]. The material of oxygen-free high
395 conductivity copper has been used to fabricate the resonator, which could improve the
396 temperature uniformity of the resonator. Therefore, the uncertainty of temperature
397 measurement has been effectively suppressed in Ref. [30], which was reduced from
398 0.96 ppm to 0.49 ppm. However, uncertainties of the other two sources, summarized in
399 Table 3, are higher than those of AGT using a spherical cavity. The random error in A_0
400 is mainly produced by the lower Q s of the cylindrical cavity, and the signal-to-noise
401 ratio of the measurements was lower than that of a spherical cavity, especially at low
402 pressures. At present, a PZT disc is used to detect the acoustic resonance signal, and the
403 response strength under low pressure can be improved by replacing it with a miniature
404 microphone in future work. Furthermore, the uncertainty of inconsistency among
405 modes is difficult to reduce because the shell motion affects the resonance signal of
406 high-frequency modes. In Ref. [30], we considered this uncertainty item as the
407 experimental standard deviation among the mean A_0 obtained from different modes.
408 However, it is not calculated in Case 3 and Case 6 of this article because only one
409 combination of modes $l_1=4$ and $l_2=2$ can actually be used in the virtual cylindrical cavity
410 to avoid the shell vibrations at high frequencies^[43]. In the future, we plan to use an
411 acoustic waveguide to drive the signal from the acoustic source to the cavity and reduce
412 the influence of resonator vibration on the inconsistency.

413 Table 3. Measurement uncertainty and their correlations for different determinations of k_B

Main uncertainty source	k_{B1}	k_{B2}	k_{B3}	k_{B4}	k_{B5}	k_{B6}	k_{B7}
	$10^6 \times u_r(k_B)$						
Random error in A_0	0.67	2.29	1.94	1.19	1.37	1.48	2.67
Inconsistency among modes	7.64	5.94	--	2.65	3.15	--	2.96

414 **4. Measurement of the Thermodynamic Temperature**415 **4.1 Thermodynamic temperature measurement limit**

416 When the Boltzmann constant is defined, AGT can be used for absolute
417 measurement of the thermodynamic temperature T based on kinetic theory of an ideal
418 gas and the squared speed of sound w_0^2 , which can be expressed by

419
$$T = \frac{w_0^2 M}{k_B \gamma_0 N_A}. \quad (22)$$

420 On the other hand, AGT can also work in a relative way as defined in Eq. (6), that
421 is to measure the ratio of the squared speed of sound at T and that at a reference
422 temperature such as T_{TPW} .

423 The apparatus and transducers previously used for determinations of k_B at the triple
424 point of water would suit thermodynamic temperature measurements below 400 K. The
425 lowest temperature of AGT is limited to the p - T region where the thermometric
426 substance is gaseous. In order to sustain high temperatures for the use of AGT, the
427 materials of the cavity and structure of the sensor are significantly important. Compared
428 with a spherical cavity, the cylindrical cavity is easier to machine and assemble, and the
429 resonant frequencies can be adjusted by varying the length of the cylinders rather than
430 the radius of the spherical cavities. Moreover, the dimension of the resonant cavity
431 determines the size of the pressure vessel and the inner space of the thermostatic system,
432 which is also important for high temperature AGT.

433 The material of the resonator is the first challenge for high temperature AGT. The
434 requirements for the material include good mechanical strength, non-magnetic,
435 chemical stability, easy to machine, and economical. At present, the types of high-

436 temperature materials mainly include metals, ceramics, and alloys. Metals such as
437 tungsten can withstand temperatures up to 3000 °C and maintain stable chemical
438 properties in contact with pure inert gas. However, it is not easy to machine tungsten
439 into a cylindrical or spherical cavity due to its high hardness. The ceramics, such as
440 alumina and boron nitride, generally can endure temperatures up to 2000 °C, and they
441 have high hardness and oxidation resistance. Nevertheless, ceramics cannot withstand
442 high pressure, they have poor thermal conductivity, and they are electrical insulators.
443 Therefore, one cannot use microwave resonances to determine the volume of a ceramic
444 cavity *in situ*. Alloys that are suitable for manufacturing a high-temperature resonator
445 have high-temperature and high-pressure resistance, stable chemical properties, and
446 easy manufacturing. One c-AGT cavity applied to test the measurement of microwave
447 resonant frequencies up to the copper point was made of Ni-Fe-Cr alloy HR120
448 (Haynes International, Kokomo, IN, USA^[49])^[25], which was capable of withstanding
449 high temperature up to 1360 K with acceptable deformation.

450 Both acoustic and microwave transducers need to be modified for measuring
451 temperature above 400 K. Acoustic waveguides (ducts) can be used to transfer the
452 acoustic signals from and to the cavity. The designs of ducts must trade off increasing
453 signal-to-noise ratios of resonance measurements against increasing frequency
454 perturbations from ducts. Ducts must be tens of centimeters long to connect a cavity in
455 a furnace with transducers at room temperature. However, sound attenuation in ducts
456 increases exponentially with length. In our setup^[25], we replaced the PZT disc used as
457 an acoustic receiver transducer in earlier work with a microphone to improve sensitivity
458 at high temperature and pressure. The microphone is placed in a miniaturized pressure
459 resistant container to ensure pressure balance on both sides of the microphone
460 diaphragm. Moreover, expanding the inner diameter of the duct is conducive to improve
461 signal to noise ratio (SNR) for the c-AGT, but it has a large perturbation to the resonator
462 and reduces the quality factor of the modes^[50]. In order to overcome the conflict
463 between SNR and mode quality factor, the concept of stepped diameter acoustic ducts
464 has been proposed. We use a narrow diameter duct connected with the resonator, and
465 the other end of it is connected to a large diameter duct to extend the length^[51]. The

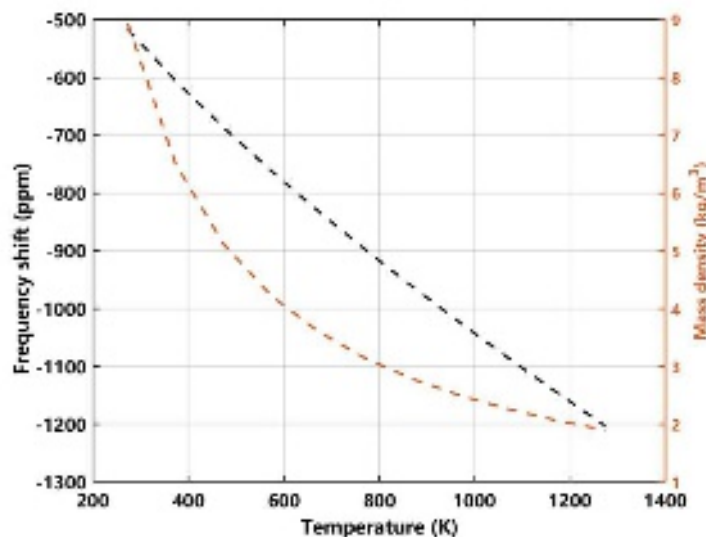
466 cavity length varies with the change of temperature due to the thermal expansion, so
467 that a microwave resonance method using home-made microwave cables can be used
468 to realize direct in-situ measurement of the length at high temperature. The center
469 conductor of coaxial cable is made from the Ni-Cr alloy (80% Ni, 20% Cr), whose
470 thermal expansion is close to that of the HR120 cavity and Inconel-625 outer conductor.
471 Furthermore, fused silica tubes and fused silica beads are used to electrically insulate
472 the center conductor from the outer shield, which satisfied the requirement of operating
473 at the copper point^[24].

474 Some other technical challenges for high-temperature AGT include an adequate
475 design of the thermostat system, the capability to preserve the gas purity, and the
476 suitable sealing of the pressure vessel. However, combined with the improvement for
477 the adaptability of c-AGT working at high temperature, the accurate measurement of
478 $T-T_{90}$ in the range of 400 K to 1358 K can be realized over an overlapping temperature
479 range with radiation thermometry.

480 **4.2 Pressure measurement limit**

481 By extrapolation of $w^2(p, T)$, measured at several pressures along an isotherm, to
482 zero pressure, we obtain $w_0^2(T)$. According to Eqs. (9) and (13), the boundary layer is
483 affected by mass density. When the temperature rises, the mass density decays with
484 constant gas pressure as shown in Fig. 9. Thus, the boundary layer effects would
485 increase with increasing temperature as shown in Fig. 9. In order to reduce the boundary
486 layer effects at high temperature, the gas pressure in the cavity should be increased to
487 avoid the decrease of density with increasing temperature. For a given density, when
488 temperature increases, the pressure increases correspondingly. It is difficult to maintain
489 the system at such a high pressure and high temperature, and the material used to
490 manufacture the resonator should have excellent pressure resistance without
491 deformation, and its bearing capacity of pressure mainly depends on the yield strength.
492 When the external force is greater than the yield strength, the material would undergo
493 permanent deformation. The yield strength of HR120 is about 45.6 KSI (375 MPa) at
494 room temperature, 25.79 KSI (177.84 MPa) at 1073 K and 9.1 KSI (62.7 MPa) at 1366

495 K. Therefore, the pressure limit of a resonator comprised of HR120 can reach the order
496 of megapascals.



497
498
499
500

Fig. 9 The calculation for frequency shift and mass density of argon variation with temperature at 505 kPa. The frequency shift is caused by the boundary layer effects at mode $l=2$ and the cavity dimension of $a=4$ cm and $L=13$ cm.

501

4.3 Influence of Working Gas

502

503

504

505

506

507

508

509

510

511

512

513

514

515

516

517

518

The working gas of AGT should be a monatomic gas, which has exactly $\gamma_0 = 5/3$, stable chemical properties and high purity, including helium (He), neon (Ne), argon (Ar), krypton (Kr) and xenon (Xe). The variation of speed of sound, resonance frequency at mode $l=2$, and quality factor with temperature for the monatomic gases has been calculated and plotted in Fig. 10 to Fig. 12. The radius and length of the cylindrical cavity used for calculation are 4 cm and 13 cm, respectively. The speed of sound and other related thermophysical properties of He, Ar, Ne below 1050 K and Kr, Xe below 1100 K used in the calculation of Fig. 10 and Fig. 12 are from Ref. [52], and the thermophysical properties for Ne from 1050 to 1300 K and Kr, Xe from 1100 K to 1300 K were obtained by extrapolating the temperature dependence of their thermodynamic properties beyond the lower temperature range in which they are available. At present, only helium and argon have been widely used in AGT. However, the resonance frequency of helium is about three times as large as that of argon for the same mode. The resonance frequencies in argon are more widely separated from the shell's natural vibrations, which is conducive to increasing measurement accuracy. Compared with helium, the application of argon can improve the measurement performance of thermodynamic temperature, especially for high-temperature

519
520
521
522
523

measurement. Moreover, the velocity of acoustic wave and resonance frequency in Ar is larger than that in Kr and Xe. Thus, Xe may be another excellent choice at high temperature.

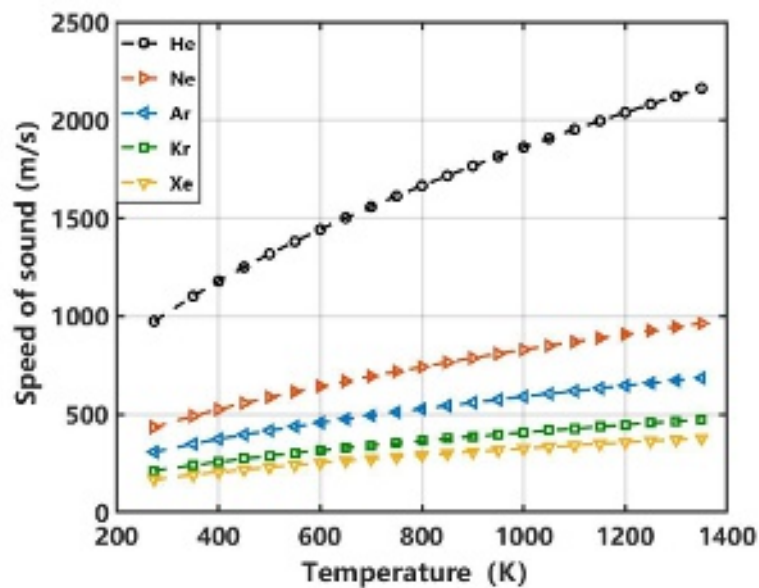


Fig. 10 Speed of sound variation with temperature for different monatomic gases at 505 kPa.

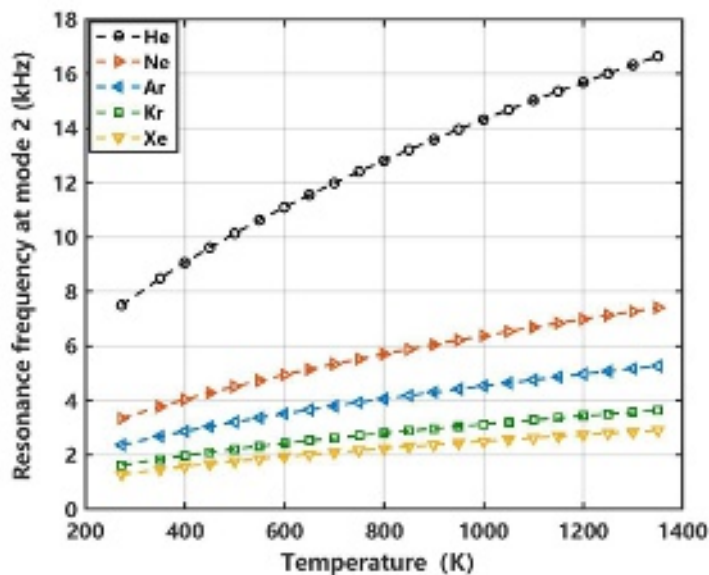
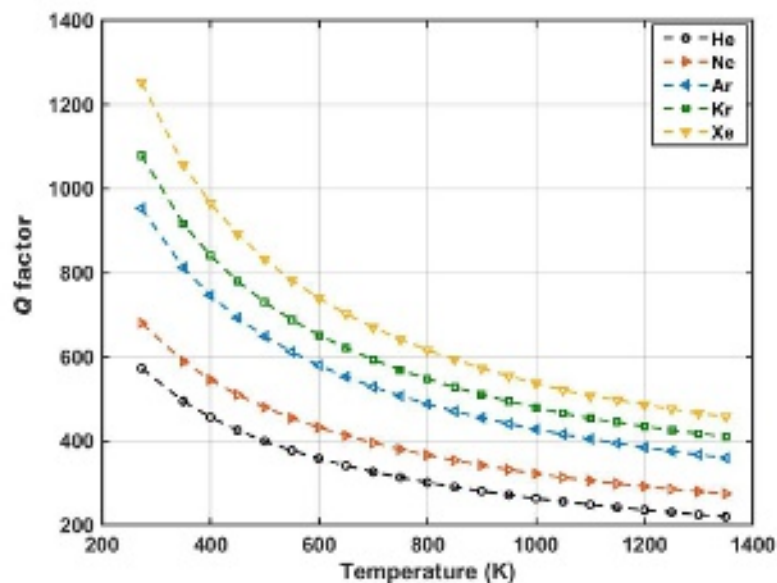
524
525
526

Fig. 11 Resonance frequency with temperature for different monatomic gases at 505 kPa for acoustic mode $l=2$ and the cavity dimension of $a=4$ cm and $L=13$ cm.



527

528

529

530

531

532

533

534

535

536

537

538

539

540

541

542

543

544

545

546

547

548

549

550

Fig. 12 The calculation of quality factors with temperature for different monatomic gases at 505 kPa for acoustic mode $l=2$ and the cavity dimension of $a=4$ cm and $L=13$ cm.

We briefly consider the advantages and disadvantages of using xenon instead of argon as the thermometric gas for AGT. The main advantage of replacing argon with xenon is the reduction of the gas resonance frequencies by a factor of 1.8. For a given mode, the gas resonance frequency varies as T/M . Thus, increasing M from 40 g/mol (argon) to 131 g/mol (xenon) can offset the gas frequency change resulting from a temperature increase from 300 K to 982 K. This flexibility could be used to avoid measurements at frequencies where particular gas modes cross particular shell modes. The main disadvantages are the added complexities of recycling the xenon and monitoring the average atomic mass of the xenon. High-temperature AGT systems continuously flow the thermometric gas through the cavity to minimize the effects of outgassing from the walls of the cavity and from the manifold and ducts that supply the gas to the cavity^[53]. The cost of highly purified argon is low enough that the argon can be discarded after it passes through the AGT cavity. The high cost of xenon requires collection of the used gas and repurifying it for reuse. Xenon is comprised of 9 stable isotopes spanning the range 124 g/mol to 136 g/mol. Accurate AGT cannot rely on a handbook value for the average atomic mass of any particular supply of xenon. Instead, the average mass can be monitored by flowing the xenon through a reference acoustic resonator maintained at a convenient fixed temperature and pressure. Such a resonator would be located just upstream of a duct that delivers xenon from a purifier to the AGT.

In contrast with helium, both xenon and argon are relatively insensitive to likely

551 impurities such as the components of air, other noble gases, and gases such as H₂ and
 552 CO that emanate from high-temperature metals, which can be seen in Table 4. Accurate
 553 values of the transport properties of xenon are available where needed for AGT.
 554 Vogel measured the viscosity of low-density xenon with a relative standard uncertainty
 555 of 0.2 % or less in the temperature range 295 K to 650 K^[54]. At the lower temperature
 556 range, Vogel's measurements are confirmed by accurate measurements made using
 557 other techniques. Hellmann *et al.* developed an *ab initio* xenon-xenon, interatomic
 558 potential that is consistent with Vogel's data^[55]. Hellmann's potential predicts accurate
 559 values of xenon's low-density viscosity, thermal conductivity, and second acoustic
 560 virial coefficient throughout the range where xenon-based AGT might be implemented.

561 Table 4. Effect of mole fraction x of impurities on w_0^2 for He, Ar, Xe

Impurity	M (g/mol)	γ_0	$\lim_{x \rightarrow 0} \frac{1}{w_0^2} \frac{d(w_0^2)}{dx}$		
			in He	in Ar	in Xe
H ₂	2	1.40	0.23	0.68	0.72
He	4	1.67	--	0.90	0.97
H ₂ O	18	1.32	-3.93	0.12	0.43
Ne	20	1.67	-4.00	0.50	0.85
N ₂ /CO	28	1.40	-6.27	0.03	0.52
O ₂	32	1.40	-7.27	-0.07	0.49
Ar	40	1.67	-9.0	--	0.69
CO ₂	44	1.40	-10	-0.4	0.40
Kr	84	1.67	-20	-1.1	0.36
Xe	131	1.67	-32	-2.3	--
Hg	201	1.67	-49	-4.0	-0.53

562 4.4 Inconsistent values of T/T_{ref}

563 Underwood's recent, preliminary measurements of c-AGT illustrated that c-AGT
 564 could determine temperature ratios with significantly greater precision than absolute
 565 temperatures^[19]. Underwood measured the frequencies of many acoustic modes of
 566 argon contained within a comparatively long, (length = 220 mm; radius = 50 mm) quasi-
 567 cylindrical cavity at 323 K and 429 K (Underwood's cavity was a cylinder with an
 568 ellipsoidal cross-section. By changing the cavity's cross-section from circular to
 569 ellipsoidal, he removed the degeneracies of certain microwave modes. This change is

This is the author's peer reviewed, accepted manuscript. However, the online version of record will be different from this version once it has been copyedited and typeset.

PLEASE CITE THIS ARTICLE AS DOI: 10.1063/1.509933

570 analogous to deforming a spherical cavity into a quasi-spherical cavity, also to remove
 571 microwave degeneracies. Therefore, we call Underwood's cavity "quasi-cylindrical"
 572 and his acoustic thermometer "qc-AGT"). The lowest frequency (1,0,0) mode at
 573 0.76 kHz is far outside the span of Fig. 13. The (1,0,0) mode couples strongly to the
 574 cavity's support and will not be discussed here. The upper panel of Fig. 13 displays a
 575 determination of an absolute temperature near 323 K from 26 modes. The measured
 576 zero-density speeds of sound $u_{\text{meas},323\text{ K}}$ are compared with the theoretical value w_{theory} .
 577 The 26 modes have the fractional standard deviation from their mean $\sigma(\Delta w/w) =$
 578 16×10^{-6} . The lower panel of Fig. 13 displays the speed of sound ratios measured using
 579 the same cavity at 323 K and 429 K. The fractional standard deviation of the 26 speed
 580 of sound ratios from their mean is $\sigma(w_{429\text{ K}}/w_{323\text{ K}}) = 6.8 \times 10^{-6}$. If the inconsistencies
 581 among the modes were random, we would expect $\sigma(w_{429\text{ K}}/w_{323\text{ K}}) = \sqrt{2} \sigma(\Delta w/w)$. In fact,
 582 $\sigma(w_{429\text{ K}}/w_{323\text{ K}})$ is less than 1/3 of this expectation. Thus, the inconsistencies at the two
 583 temperatures are highly correlated. If $\sigma(w_{429\text{ K}}/w_{323\text{ K}})$ dominated the uncertainty of a
 584 determination of 429 K, the determination's uncertainty would be somewhat larger than
 585 $2 \times 6.8 \times 10^{-6} \times 429\text{ K} = 5.8\text{ mK}$. This uncertainty is much smaller than 10.1 mK of the
 586 estimated error in ITS-90 at 429 K^[20]. We expect that the high correlation among these
 587 modes persists to high temperatures, where the errors in ITS-90 are larger.
 588

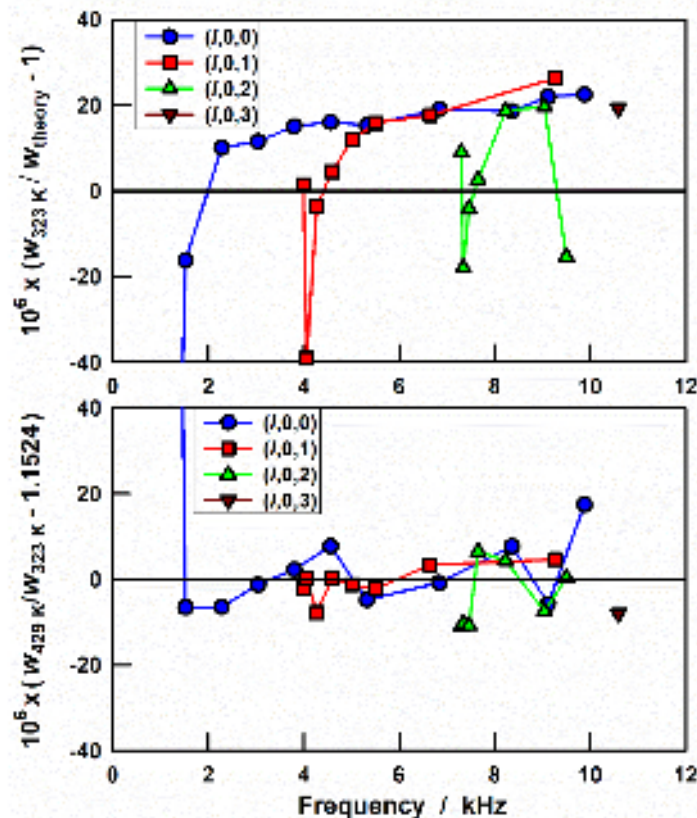


Fig. 13 Top: Measurements of w made with 26 modes of a quasi-cylindrical cavity are compared with theory at 323 K^[19]. The fractional standard deviation from the mean of the 26 modes is $\sigma(\Delta w/w) = 16 \times 10^{-6}$. Bottom: Speed of sound ratios determined separately for each mode of the same resonator at 323 K and 429 K. For the 26 modes plotted, $\sigma(w_{429 \text{ K}}/w_{323 \text{ K}}) = 6.8 \times 10^{-6}$. The speed of sound ratios are more consistent than the values of $(w_{\text{meas}}/w_{\text{theory}} - 1)$.

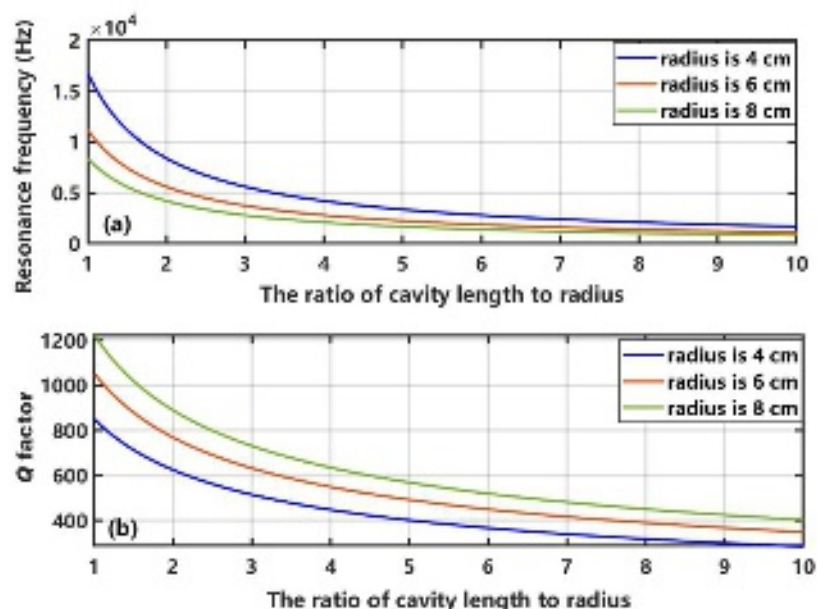
4.5 Dimensions of the resonator

With increasing temperature, the resonance frequency of the cavity will increase and meanwhile the quality factor will decrease at a stable pressure. The dimensions of resonator can affect the boundary layer, so that the performance of high-temperature measurement can be improved by optimizing the dimensions of resonator. The dimensional optimization of the cylindrical resonator mainly involves optimizing the ratio of length to radius. According to the equations in Ref. [32], the relationships of resonance frequency and Q (only considered the boundary layers effects) to the ratio of cavity length to radius at 1300 K and 505 kPa have been calculated for mode $l=2$ and showed in Fig. 14(a) and Fig. 14(b), respectively. The resonance frequency decreases with increasing ratio of cavity length to radius, and the attenuation is not obvious when the ratio is greater than 4. The resonance frequency increases with rising temperature and decreases with increasing radius because of the growth of length. However, the Q factor will decrease with the increase of the ratio. A c-AGT with a large volume is

This is the author's peer reviewed, accepted manuscript. However, the online version of record will be different from this version once it has been copyedited and typeset.

589
590
591
592
593
594
595
596
597
598
599
600
601
602
603
604
605
606
607
608

609 difficult to maintain at a uniform temperature at high temperatures and it is difficult to
610 machine and install. We prefer to use the cylindrical resonator with the ratio of cavity
611 length to radius between 2 and 4.



612

613

614

615

616

617

618

619

620

621

622

623

624

625

626

627

628

629

630

631

632

633

634

635

636

637

638

639

640

Fig. 14 The calculation results for properties of cylindrical cavity under different ratio of length to radius. (a) Variation of resonance frequencies at mode $l=2$ under different radius. (b) Variation of Q factors under different radius.

5. Conclusion

We illustrate the performance of c-AGT for measuring the Boltzmann constant and thermodynamic temperature, respectively. From the present measurement, c-AGT could determine thermodynamic temperature ratios with significantly greater precision than that determined for absolute temperatures. The T uncertainty from c-AGT is lower than the error of ITS-90. With high-temperature acoustic and microwave waveguides and high temperature alloys, c-AGT can withstand high temperature up to the copper point. For the realization of the definition of the kelvin, cylindrical acoustic gas thermometry can play a more important role in thermodynamic temperature measurement in the future.

627 Acknowledgments

628 NIM's research was supported by the National Key R&D Program of China (no.
629 2021YFF0603703) and the National Natural Science Foundation of China (no.
630 52176170). Li Xing thanks the support from China Postdoctoral Science Foundation
631 (No. 2021M703049). We thank Robin Underwood for providing the data in Fig. 13. In
632 order to describe materials and procedures adequately, such as Ni-Fe-Cr alloy HR120,
633 it is occasionally necessary to identify commercial products by manufacturers' name or
634 label. In no instance does such identification imply endorsement by the National
635 Institute of Metrology of China or by the National Institute of Standards and
636 Technology of the USA, nor does it imply that the particular product or equipment is
637 necessarily the best available for the purpose.

638 6. Author Declarations

639 6.1 Conflict of interest

640 The authors have no conflicts to disclose.

641 References

- 642 [1] R. L. Rusby, R. P. Hudson, M. Durieux, J. F. Schooley, P. P. M. Steur, and C. A.
643 Swenson, "Thermodynamic basis of the ITS-90," *Metrologia* **28**, 9 (1991).
- 644 [2] T. J. Quinn, T. Chandler, and A. R. Colclough, "A new determination of the gas
645 constant by an acoustical method," *Nature* **250**, 218 (1974).
- 646 [3] M. R. Moldover, J. B. Mehl, and M. Greenspan, "Gas-filled spherical resonators:
647 Theory and experiment," *J. Acoust. Soc. Am.* **79**, 253 (1986).
- 648 [4] K. A. Gillis, M. R. Moldover, and A. R. H. Goodwin, "Accurate acoustic
649 measurements in gases under difficult conditions," *Rev. Sci. Instrum.* **62**, 2213 (1991).
- 650 [5] I. M. Mills, P. J. Mohr, T. J. Quinn, B. N. Taylor, and E. R. Williams, "Redefinition
651 of the kilogram, ampere, kelvin and mole: a proposed approach to implementing CIPM
652 recommendation 1 (CI-2005)," *Metrologia* **43**, 227 (2006).
- 653 [6] J. Fischer *et al.*, "The Boltzmann project," *Metrologia* **55** (2018).
- 654 [7] M. R. Moldover, J. P. M. Trusler, T. J. Edwards, J. B. Mehl, and R. S. Davis,
655 "Measurement of the universal gas constant R using a spherical acoustic resonator,"
656 *Phys. Rev. Lett.* **60**, 249 (1988).
- 657 [8] L. Pitre, C. Guianvarc'h, F. Sparasci, A. Guillou, D. Truong, Y. Hermier, and M. E.
658 Himbert, "An improved acoustic method for the determination of the Boltzmann
659 constant at LNE-INM/CNAM," *C. R. Phys.* **10**, 835 (2009).
- 660 [9] M. R. Moldover, S. J. Boyes, and A. R. H. Goodwin, "Thermodynamic

- 661 temperatures of the triple points of mercury and gallium and in the interval 217 K to
662 303 K,” J. Res. Natl. Inst. Stand. Technol. **104**, 11 (1999).
- 663 [10]G. F. Strouse, D. R. Defibaugh, M. R. Moldover, and D. C. Ripple, “Progress in
664 primary acoustic thermometry at NIST: 273 K to 505 K,” AIP Conf. Proc. **684**, 31
665 (2003).
- 666 [11]D. C. Ripple, G. F. Strouse, and M. R. Moldover, “Acoustic thermometry results
667 from 271 to 552 K,” Int. J. Thermophys. **28**, 1789 (2007).
- 668 [12]R. Underwood, M. de Podesta, G. Sutton, L. Stanger, R. Rusby, P. Harris, P.
669 Morantz, and G. Machin, “Further estimates of $(T-T_{90})$ close to the triple point of water,”
670 Int. J. Thermophys. **38**, 1 (2017).
- 671 [13]M. B. Ewing and J. P. M. Trusler, “Primary acoustic thermometry between $T=90$ K
672 and $T=300$ K,” J. Chem. Thermodyn. **32**, 1229 (2000).
- 673 [14]G. Benedetto, R. M. Gavioso, R. Spagnolo, P. Marcarino, and A. Merlone,
674 “Acoustic measurements of the thermodynamic temperature between the triple point of
675 mercury and 380 K,” Metrologia **41**, 74 (2004).
- 676 [15]L. Pitre, M. R. Moldover, and W. L. Tew, “Acoustic thermometry: new results from
677 273 K to 77 K and progress towards 4 K,” Metrologia **43**, 142 (2006).
- 678 [16]K. Zhang, X. J. Feng, J. Zhang, and Y. Duan, “Determination of $T-T_{90}$ from 234 K
679 to 303 K by acoustic thermometry with a cylindrical resonator,” Metrologia **57**, 024004
680 (2020).
- 681 [17]C. Gaiser and B. Fellmuth, “Highly-accurate second-virial-coefficient values for
682 helium from 3.7 K to 273 K determined by dielectric-constant gas thermometry,”
683 Metrologia **58**, 015013 (2021).
- 684 [18]C. Gaiser *et al.*, “2022 Update for the Differences Between Thermodynamic
685 Temperature and ITS-90 Below 335 K,” J. Phys. Chem. Ref. Data **51**, 043105 (2022).
- 686 [19]H. C. McEvoy *et al.*, “Methodologies and uncertainty estimates for $T-T_{90}$
687 measurements over the temperature range from 430 K to 1358 K under the auspices of
688 the EMPIR InK2 project,” Meas. Sci. Technol. **32**, 035001 (2020).
- 689 [20]J. Fischer, M. De Podesta, K. D. Hill, M. Moldover, L. Pitre, R. Rusby, P. Steur, O.
690 Tamura, R. White, and L. Wolber, “Present estimates of the differences between
691 thermodynamic temperatures and the ITS-90,” Int. J. Thermophys. **32**, 12 (2011).
- 692 [21]L. Pitre, F. Sparasci, D. Truong, A. Guillou, L. Risegari, and M. E. Himbert,
693 “Measurement of the Boltzmann constant k_B using a quasi-spherical acoustic resonator,”
694 Int. J. Thermophys. **32**, 1825 (2011).
- 695 [22]M. de Podesta, R. J. Underwood, G. Sutton, P. Morantz, P. Harris, D. F. Mark, F.
696 M. Stuart, G. Vargha, and G. Machin, “A low-uncertainty measurement of the
697 Boltzmann constant,” Metrologia **50**, 354 (2013).
- 698 [23]R. M. Gavioso, D. Madonna Ripa, P. P. M. Steur, C. Gaiser, D. Truong, C.
699 Guianvarc’h, P. Tarizzo, F. M. Stuart, and R. Dematteis, “A determination of the molar
700 gas constant R by acoustic thermometry in helium,” Metrologia **52**, S274 (2015).
- 701 [24]X. J. Feng, K. A. Gillis, M. R. Moldover, and J. B. Mehl, “Microwave-cavity
702 measurements for gas thermometry up to the copper point,” Metrologia **50**, 219 (2013).

- 703 [25]K. Zhang, X. J. Feng, K. Gillis, M. Moldover, J. T. Zhang, H. Lin, J. F. Qu, and Y.
704 N. Duan, “Acoustic and microwave tests in a cylindrical cavity for acoustic gas
705 thermometry at high temperature,” *Phil. Trans. Roy. Soc. A* **374**, 20150049 (2016).
- 706 [26]P. J. Mohr, D. B. Newell, B. N. Taylor, and E. Tiesinga, “Data and analysis for the
707 CODATA 2017 special fundamental constants adjustment,” *Metrologia* **55**, 125 (2018).
- 708 [27]L. Pitre *et al.*, “New measurement of the Boltzmann constant k by acoustic
709 thermometry of helium-4 gas,” *Metrologia* **54**, 856 (2017).
- 710 [28]M. De Podesta, D. F. Mark, R. C. Dymock, R. Underwood, T. Bacquart, G. Sutton,
711 S. Davidson, and G. Machin, “Re-estimation of argon isotope ratios leading to a revised
712 estimate of the Boltzmann constant,” *Metrologia* **54**, 683 (2017).
- 713 [29]F. J. Pérez-Sanz, J. J. Segovia, M. C. Martín, M. A. Villamañán, D. del Campo, and
714 C. García, “Progress towards an acoustic determination of the Boltzmann constant at
715 CEM-UVa,” *Metrologia* **52**, S257 (2015).
- 716 [30]X. J. Feng, J. Zhang, H. Lin, K. A. Gillis, J. B. Mehl, M. R. Moldover, K. Zhang,
717 and Y. N. Duan, “Determination of the Boltzmann constant with cylindrical acoustic
718 gas thermometry: new and previous results combined,” *Metrologia* **54**, 748 (2017).
- 719 [31]J. T. Zhang, H. Lin, J. P. Sun, X. J. Feng, K. A. Gillis, and M. R. Moldover,
720 “Cylindrical acoustic resonator for the re-determination of the Boltzmann constant,” *Int.*
721 *J. Thermophys.* **31**, 1273 (2010).
- 722 [32]J. T. Zhang, H. Lin, X. J. Feng, J. P. Sun, K. A. Gillis, M. R. Moldover, and Y. Y.
723 Duan, “Progress toward redetermining the Boltzmann constant with a fixed-path-length
724 cylindrical resonator,” *Int. J. Thermophys.* **32**, 1297 (2011).
- 725 [33]H. Lin, X. J. Feng, K. A. Gillis, M. R. Moldover, J. T. Zhang, J. P. Sun, and Y. Y.
726 Duan, “Improved determination of the Boltzmann constant using a single, fixed-length
727 cylindrical cavity,” *Metrologia* **50**, 417 (2013).
- 728 [34]B. F. Billing and T. J. Quinn, “Temperature measurement, 1975: invited and
729 contributed papers from the European Conference on Temperature Measurement held
730 at the National Physical Laboratory, Teddington, 9-11 April 1975,” *Phys. Bull.* **27**, 406
731 (1976).
- 732 [35]T. J. Quinn, *Temperature* (Academic Press, London, 1983).
- 733 [36]E. Tiesinga, P. J. Mohr, D. B. Newell, and B. N. Taylor, “CODATA recommended
734 values of the fundamental physical constants: 2018,” *J. Phys. Chem. Ref. Data* **50**,
735 033105 (2021).
- 736 [37]F. Sharipov and M. R. Moldover, “Energy accommodation coefficient extracted
737 from acoustic resonator experiments,” *J. Vac. Sci. Technol. A* **34**, 061604 (2016).
- 738 [38]M. R. Moldover, R. M. Gavioso, J. B. Mehl, L. Pitre, M. de Podesta, and J. T.
739 Zhang, “Acoustic gas thermometry,” *Metrologia* **51**, R1 (2014).
- 740 [39]H. Lin, K. A. Gillis, and J. T. Zhang, “Characterization of piezoelectric ceramic
741 transducer for accurate speed-of-sound measurement,” *Int. J. Thermophys* **31**, 1234
742 (2010).
- 743 [40]K. A. Gillis, H. Lin, and M. R. Moldover, “Perturbations from ducts on the modes
744 of acoustic thermometers,” *J. Res. Natl. Inst. Stand. Technol.* **114**, 263 (2009).

- 745 [41] M. B. Ewing, A. A. Owusu, and J. P. M. Trusler, "Second acoustic virial coefficients
746 of argon between 100 and 304 K," *Physica A* **156**, 899 (1989).
- 747 [42] M. B. Ewing and A. R. H. Goodwin, "An apparatus based on a spherical resonator
748 for measuring the speed of sound in gases at high pressures. Results for argon at
749 temperatures between 255 K and 300 K and at pressures up to 7 MPa," *J. Chem.*
750 *Thermodyn.* **24**, 531 (1992).
- 751 [43] X. J. Feng, H. Lin, K. A. Gillis, M. R. Moldover, and J. T. Zhang, "Test of a virtual
752 cylindrical acoustic resonator for determining the Boltzmann constant," *Metrologia* **52**,
753 S343 (2015).
- 754 [44] K. Zhang, X. J. Feng, J. T. Zhang, H. Lin, Y. N. Duan, and Y. Y. Duan, "Microwave
755 measurements of the length and thermal expansion of a cylindrical resonator for
756 primary acoustic gas thermometry," *Meas. Sci. Technol.* **28**, 015006 (2016).
- 757 [45] G. Sutton, R. Underwood, L. Pitre, M. de Podesta, and S. Valkiers, "Acoustic
758 resonator experiments at the triple point of water: first results for the Boltzmann
759 constant and remaining challenges," *Int. J. Thermophys.* **31**, 1310 (2010).
- 760 [46] J. J. Segovia, D. Lozano-Martín, M. C. Martín, C. R. Chamorro, M. A. Villamañán,
761 E. Pérez, C. G. Izquierdo, and D. del Campo, "Updated determination of the molar gas
762 constant R by acoustic measurements in argon at UVa-CEM," *Metrologia* **54**, 663
763 (2017).
- 764 [47] A. F. Estrada-Alexanders, O. Guzmán, and B. Pérez-Vidal, "High-precision virial
765 coefficients of argon and carbon dioxide from integration of speed of sound data in the
766 pressure-temperature domain," *Mol. Phys.* **110**, 1349 (2012).
- 767 [48] B. Jäger, R. Hellmann, E. Bich, and E. Vogel, "*Ab initio* virial equation of state for
768 argon using a new nonadditive three-body potential," *J. Chem. Phys.* **135**, 084308
769 (2011).
- 770 [49] J. Fischer *et al.*, "Uncertainty budgets for realisation of scales by radiation
771 thermometry," International Bureau of Weights and Measures CCT/03-03 (2003).
- 772 [50] H. Lin, X. J. Feng, and J. T. Zhang, "Perturbation measurement of waveguides for
773 acoustic thermometry," *AIP Conf. Proc.* **1552**, 39 (2013).
- 774 [51] H. H. Chen, X. J. Feng, H. Lin, J. T. Zhang, C. Ren, and K. J. Wang, "Study on
775 optimal design of acoustic conduit in gas acoustic thermometer," *Acta Metrologica*
776 *Sinica* **40**, 7 (2019).
- 777 [52] E. W. Lemmon, I. H. Bell, M. L. Huber, M. O. McLinden, NIST Standard
778 Reference Database 23: Reference Fluid Thermodynamic and Transport Properties-
779 REFPROP, Version 10.0, National Institute of Standards and Technology, Standard
780 Reference Data Program, Gaithersburg, <https://doi.org/10.18434/T4/1502528>, 2018.
- 781 [53] D. C. Ripple, D. R. Defibaugh, M. R. Moldover, and G. F. Strouse, "Techniques
782 for primary acoustic thermometry to 800 K," *AIP Conf. Proc.* **684**, 25 (2003).
- 783 [54] E. Vogel, "The viscosities of dilute Kr, Xe, and CO₂ revisited: New experimental
784 reference data at temperatures from 295 K to 690 K," *Int. J. Thermophys.* **37**, 1 (2016).
- 785 [55] R. Hellmann, B. Jäger, and E. Bich, "State-of-the-art *ab initio* potential energy
786 curve for the xenon atom pair and related spectroscopic and thermophysical properties,"
787 *J. Chem. Phys.* **147**, 034304 (2017).